SPICAM: Studying the Global Structure and Composition of the Martian Atmosphere

J.-L. Bertaux[1], D. Fonteyn[2], O. Korablev[3], E. Chassefière[4], E. Dimarellis[1], J.P. Dubois[1], A. Hauchecorne[1], F. Lefèvre[1], M. Cabane[1], P. Rannou[1], A.C. Levasseur-Regourd[1], G. Cernogora[1], E. Quemerais[1], C. Hermans[2], G. Kockarts[2], C. Lippens[2], M. De Maziere[2], D. Moreau[2], C. Muller[2], E. Neefs[2], P.C. Simon[2], F. Forget[4], F. Hourdin[4], O. Talagrand[4], V.I. Moroz[3], A. Rodin[3], B. Sandel[5] & A. Stern[6]

[1]*Service d'Aéronomie du CNRS, F-91371, Verrières-le-Buisson, France*
Email: jean-loup.bertaux@aerov.jussieu.fr
[2]*Belgian Institute for Space Aeronomy, 3 av. Circulaire, B-1180 Brussels, Belgium*
[3]*Space Research Institute (IKI), 84/32 Profsoyuznaya, 117810 Moscow, Russia*
[4]*Laboratoire de Météorologie Dynamique, 4 place Jussieu, F-75252 Paris Cedex 05, Paris, France*
[5]*Lunar and Planetary Laboratory, 901 Gould Simpson Building, Univ. of Arizona, Tucson, AZ 85721, USA*
[6]*SouthWest Research Institute, Geophysics, Astrophysics and Planetary Science, 1050 Walnut Ave., Suite 400, Boulder, CO 80302-5143, USA*

The SPICAM (SPectroscopy for the Investigation of the Characteristics of the Atmosphere of Mars) instrument consists of two spectrometers. The UV spectrometer addresses key issues about ozone and its H_2O coupling, aerosols, the atmospheric vertical temperature structure and the ionosphere. The IR spectrometer is aimed primarily at H_2O abundances and vertical profiling of H_2O and aerosols. SPICAM's density/temperature profiles will aid the development of meteorological and dynamical atmospheric models from the surface up to 160 km altitude. UV observations of the upper atmosphere will study the ionosphere and its direct interaction with the solar wind. They will also allow a better understanding of escape mechanisms, crucial for insight into the long-term evolution of the atmosphere.

1. Introduction

1.1 SPICAM goals

SPICAM (Fig. 1), a lightweight (4.7 kg) UV-IR spectrometer on the Mars Express orbiter, is dedicated to recovering most of the atmospheric science that was lost with Mars-96 and its set of SPICAM sensors. The new configuration of SPICAM includes a 2-channel optical sensor (3.8 kg) and an electronics block (0.9 kg). The UV spectrometer (118-320 nm, resolution 0.8 nm) is dedicated to nadir viewing, limb viewing and vertical profiling by stellar and solar occultation. It addresses key issues about ozone and the H_2O coupling, aerosols, atmospheric vertical temperature structure and the ionosphere. The near-IR spectrometer (1.0-1.7 µm, resolution 0.5-1.2 nm) is aimed primarily at nadir measurements of H_2O abundances, and at vertical profiling of H_2O and aerosols by solar occultation. A simple data processing unit (0.9 kg) provides the interface with the spacecraft.

For nadir observations, SPICAM UV is essentially an ozone detector, measuring the strongest O_3 absorption band at 250 nm in the solar light scattered from the ground. In its stellar occultation mode, the UV sensor will measure the vertical profiles of CO_2, temperature, O_3, clouds and aerosols. The density/temperature profiles will constrain and aid in developing the meteorological and dynamical atmospheric models from the surface and up to 160 km in the atmosphere. This is

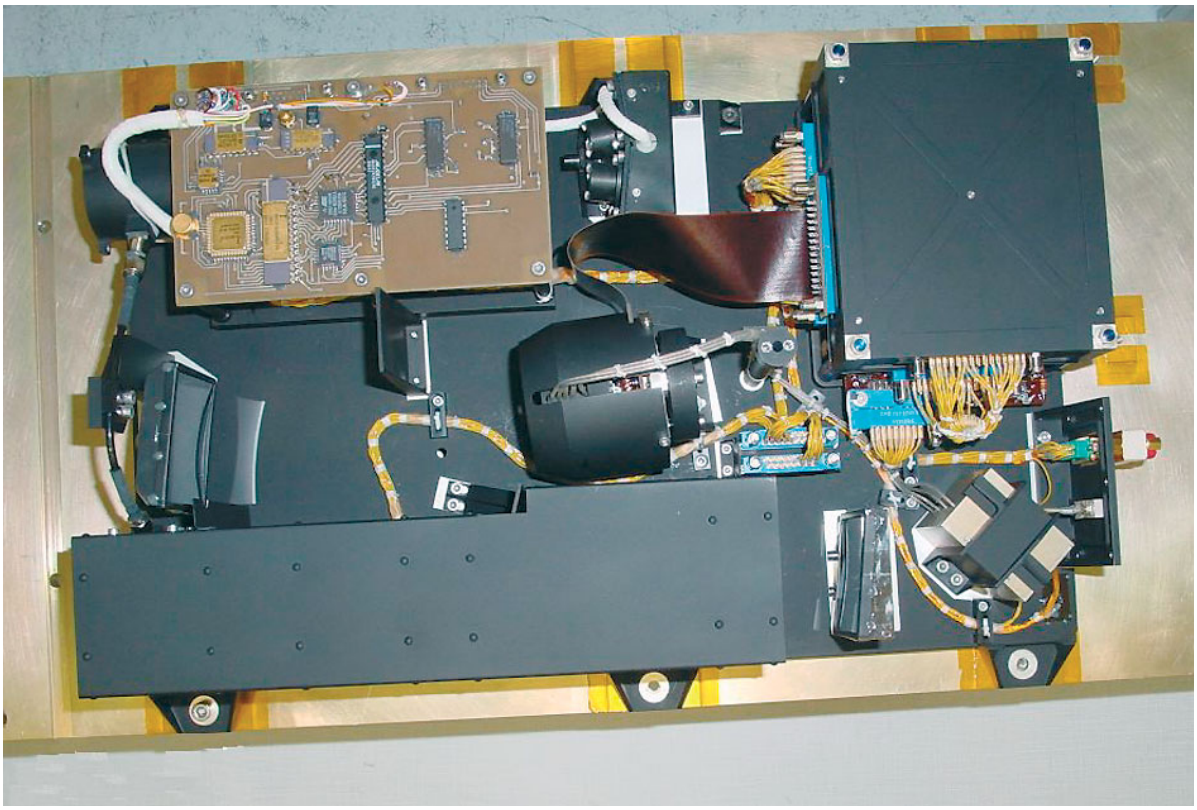

Fig. 1. Flight Model Sensor Unit of SPICAM viewed from above. The IR AOTF spectrometer is at top; the UV spectrometer is at bottom. The common optical axis points to the left. For the UV spectrometer, the light enters the mechanical baffle (black), is focused by a parabolic mirror (bottom right) through a slit, then dispersed by the grating (middle left), to be refocused on the intensified CCD Detector (at centre).

essential for future missions that rely on aerocapture and aerobraking. UV observations of the upper atmosphere will allow studies of the ionosphere through the emissions of CO, CO^+ and CO_2^+, and its direct interaction with the solar wind. Also, it will allow a better understanding of escape mechanisms and estimates of their magnitude, crucial for insight into the long-term evolution of the atmosphere.

SPICAM's near-IR sensor, employing the pioneering technology of an acousto-optical tunable filter (AOTF), is dedicated to the measurement of water vapour column abundance in the IR simultaneously with ozone measured in the UV. It will be achieved with a much lower telemetry budget than the mission's Planetary Fourier Spectrometer. In solar occultation mode, this channel will study the vertical structures of H_2O, CO_2 and aerosols.

1.2 Background

Observations during the 18th century showed that light from the star Spica decreased abruptly during occultations by the Moon. It was concluded that the Moon has no atmosphere because, otherwise, refraction would have produced a progressive dimming of the star. The SPICAM acronym is a tribute to this early use of stellar occultation.

In the Earth's atmosphere, the occultation technique has been used to measure O_3 since the 1970s. Only one or two wavelengths were observed at a time in the early attempts, making identification of the absorber species uncertain. With the advent of multi-pixel detectors, the absorbing species can be safely identified by their spectral signatures. It also offers the potential to discover new, unexpected species in the atmosphere. The method of absorptive occultation spectroscopy is reviewed in Roscoe et al. (1994) and Smith & Hunten (1990). For terrestrial stratospheric research, it has become the most advanced method for long-term monitoring of ozone. In the IR, the most remarkable results are those of the ATMOS/Atlas Space Shuttle experiment, which provided a set of high-resolution IR spectra of the terrestrial

atmosphere. In the UV-visible, NASA's SAGE-3 is using full-wavelength coverage of the Sun. Onboard Envisat, SCIAMACHY (Scanning Imaging Absorption Spectrometer for Atmospheric Chartography) is performing solar occultation and nadir observations, and the GOMOS (Global Ozone Monitoring by Occultations of Stars) instrument is dedicated to the monitoring of ozone and other species by stellar occultations. SPICAM's methodology is clearly in line with the most advanced instrumentation for studying Earth's atmosphere.

The only solar occultation measurements so far of Mars from spacecraft were performed during the Phobos mission using the Auguste instrument (Blamont et al., 1989; Krasnopolsky et al., 1989). Though the Phobos mission was not fully successful, the solar occultation observations lasted more than a month, resulting in an important improvement of our knowledge of the martian water vapour profile (Krasnopolsky et al., 1991; Rodin et al., 1997), aerosol vertical distribution (Chassefière et al., 1992; Korablev et al., 1993) and ozone distribution (Blamont & Chassefière, 1993).

The promising results from the Phobos mission were not fully developed because of the failure of the Mars-96 mission, where the SPICAM set of sensors (total 46 kg) was dedicated to studying the martian atmosphere. The 4.7 kg SPICAM 'Light' of Mars Express will recover most of the science of SPICAM/Mars-96. The considerable mass saving was achieved by sacrificing all the visible part of the spectrum and by suppressing all redundancy between the two sensors. Also, using the spacecraft for pointing removes the need for pointing platforms and devices. The proposal for this SPICAM included a separate solar occultation IR sensor (SOIR), inherited from the solar package of SPICAM/Mars-96. This 3.8 kg sensor consisted of a grating spectrometer (1.2-4.8 µm, resolution 0.4-1 nm) for vertical profiling during solar occultations of H_2O, CO_2, CO and aerosols and exploration of carbon compounds (Bertaux et al., 2001). Owing to the severe mass constraints of Mars Explorer, this sensor was deleted at the development stage, and replaced by the extremely lightweight near-IR spectrometer based on AOTF technology. The consequences for the scientific return are discussed below.

2. Scientific Objectives

The tenuity of the CO_2 martian atmosphere and the partial transparency to solar UV results in intense photochemical activity, possibly including photocatalytic processes at the surface or on aerosols. Although the global mechanism of atmospheric chemical stability proposed at the beginning of the 1970s (Parkinson & Hunten, 1972) is generally accepted, no substantial progress in modelling has been made in the last 20 years. Understanding martian atmospheric chemistry is of fundamental importance for characterising the history of Mars (escape of species to space, atmosphere/surface interactions such as oxidation) as well as for comparison with terrestrial processes (chemistry/dynamics coupling, possible role of heterogeneous chemistry). Besides chemical processes, addressing the key problems of the martian climate includes understanding the transport of radiatively active aerosols, microphysics of clouds, regolith/atmosphere water exchange and wave activity in the atmosphere. So far, most of the data on the composition and structure of the martian atmosphere relate to the total content of the species, with very little information on the vertical profiles of aerosols, ozone, water vapour and other trace gases. SPICAM focuses on the determination of atmospheric characteristics from the surface up to 160 km altitude. SPICAM's main objectives are defined in the following five subsections.

2.1 Three-dimensional studies related to atmospheric chemical stability

An important step in improving our knowledge of martian photochemistry is the validation of the currently accepted scheme of chemical atmospheric stability, originally proposed by Parkinson & Hunten (1972). To explain the CO_2 stability, this scheme invokes odd-hydrogen photochemical species that catalyse the recombination of CO and O. These catalytic reactions are so efficient that O_2 and CO appear in the

atmosphere only in very small amounts – the observed quantities are around 0.1%. The photochemistry scheme is complicated by the amount of water, which is highly variable. The ozone density is directly connected to HO_x radicals, which are the product of water vapour dissociation. Early photochemical theories (McElroy & Donahue, 1972; Parkinson & Hunten, 1972) are confirmed by more recent photochemistry models (Nair et al., 1994; Krasnopolsky, 1993). SPICAM provides the opportunity to validate the stability scheme through simultaneous measurements of water vapour, ozone and temperature with a good vertical resolution, as well as of their diurnal, seasonal and latitudinal variations.

Since the water vapour cycle is one of the three important atmospheric cycles (the others being the dust and CO_2 cycles), the present distribution and annual variability of water reflect both current and past climate processes. In the 1970s, the Mars Atmosphere Water Detector (MAWD) on the Viking orbiters mapped for the first time the column abundance of water, for 1.5 martian years. Maximum water content is observed above the North Pole in summer as a consequence of the sublimation of the polar cap. In addition, the exchange of water between the atmosphere and the regolith is likely on both diurnal and seasonal bases. The pore volume of the martian regolith is substantial and implies that a large part of it can act as a water reservoir. Using solar occultations, the IR channel will accurately measure the vertical structure of water vapour in the atmosphere, allowing these important water-exchange processes to be assessed.

The key processes controlling the vertical distribution of water vapour on Mars are likely to be large-scale transport, turbulent mixing, the microphysics of nucleation, growth and sedimentation of ice crystals, and photochemical reactions. Moreover, the water vapour profile is closely connected to the temperature structure (both dynamic and radiative) through saturation water pressure. However, the available data do not allow an adequate determination of the detailed spatial and seasonal variations in the vertical distribution of water.

Observations of other trace species will also be important in understanding the behaviour of atmospheric water. One of these trace gases is ozone. The ozone vertical profile is governed mainly by the abundance of water vapour and it is widely acknowledged that there is a strong anti-correlation between water vapour and atmospheric ozone (Barth et al., 1973). Even if the atmospheric ozone content is low, this constituent is important for characterising the physico-chemical structure of the atmosphere. Only marginal information is available about the vertical distribution of ozone: a layer has been tentatively detected in the middle atmosphere by solar occultation (Blamont & Chassefière, 1993). SPICAM will fill this gap by measuring ozone profiles using stellar occultations in the UV.

Finally, SPICAM's nadir-viewing capability will allow the mapping of ozone column density. In conjunction with the column density of water vapour, as measured by SPICAM's IR channel or other Mars Express instruments, this will permit detailed global scale correlation studies. It should be emphasised that, so far, there is no direct experimental correlation between H_2O and ozone distributions, owing to the lack of simultaneous measurements. Some correspondence of high ozone near the poles with H_2O derived from temperature-dependent water pressure was found from Mariner-9 ozone (Barth et al., 1973) and temperature measurements (Barth et al., 1992). SPICAM offers the first possibility of firmly establishing this correlation.

2.2 Atmospheric escape

The efficiency of atmospheric escape is strongly mass-dependent, and it is quite significant for hydrogen and deuterium. The geological evidence for running water on the martian surface in the distant past is well established, but the total amount of water and the periods of activity are still controversial (Carr, 1996). Observation of D/H is thus particularly important for reconstructing the history of water on Mars. For this, the fundamental 3.7 µm HDO band was to be studied with the SOIR solar occultation channel.

An important goal of atmospheric studies is the characterisation of escape processes, which are believed to have played an important role in climate evolution. The main processes of removing mass from the atmosphere are the sputtering of atmospheric species by oxygen pick-up ions at the exobase level, and photochemical escape (Kass & Yung, 1995; Jakosky et al., 1994). The close coupling of all the atmospheric layers makes it interesting to measure the profiles of hydrogen, carbon and oxygen species in the lower ionosphere, where strong vertical fluxes of these species are supposed to take place. SPICAM will observe resonant scattering emissions of H, C and O in the altitude range 100-200 km, as well as some fluorescence bands of CO and major ions (CO_2^+, CO^+). This altitude range, an essential interface region between the low atmosphere and the upper ionosphere (where escape occurs through direct interaction with the solar wind), cannot be studied with *in situ* measurements because of the pericentre altitude of 300 km. UV glow measurements by SPICAM should provide information about thermospheric ion-neutral chemistry and related vertical fluxes of chemical species at the top of the atmosphere, as well as about their diurnal and seasonal variations.

2.3 Surface/atmosphere chemical interaction; mapping of the atmospheric and surface oxidant

The level of biologically lethal UV arriving at the surface of Mars is controlled by the vertical column of ozone, which is itself controlled by H_2O, according to present photochemistry models. These models also predict the presence of O, H_2O_2, HO_2, OH molecules and radicals, which are extremely reactive with the surface. Together with ozone, they are the main factors destroying any organic molecule that could be present on the surface (Stoker & Bullock, 1997). This radiative-chemical environment of exobiological significance will be evaluated at a variety of locations, latitudes and seasons, thanks to the polar orbit of Mars Express and its martian-year lifetime. A photochemistry model validated by the consistency of various measurements makes it possible to extrapolate back in time and to assess more safely the conditions constraining the development of life on Mars.

More than 25 years ago, the Viking life detection experiments proved that the martian soil is extraordinarily oxidising. The evolution of CO_2 from the labelled release experiment is consistent with the presence of a thermally labile oxidant. Detection and characterisation of the chemical and physical nature of this powerful oxidant is therefore of great interest not only from an exobiological point of view but also for studying exchanges between the atmosphere and the regolith on Mars. In the thin and cold atmosphere, photochemical reactions between traces of water and solar UV probably lead to the production of H_2O_2 which, in turn, can condense onto soil grains and airborne dust. Hydrogen peroxide has not yet been detected in the Martian atmosphere. A tentative detection/upper limit experiment in millimetric waves was carried out using the Interferomètre Radio Astronomique Millimétrique (IRAM) telescope (Moreau et al., 1998). Estimating the total abundance of this constituent might be feasible using SPICAM's UV channel.

2.4 Wave activity in the middle atmosphere and thermosphere

Theory predicts that the temperature structure of the thermosphere above 120 km is dominated by the balance between EUV heating, non-LTE cooling and molecular diffusion. In the middle atmosphere (40-120 km), the vertical structure is determined primarily by non-LTE solar heating and radiative cooling in the absorption bands of CO_2, and by solar EUV heating at higher levels. The thermal structure is modified by the circulation driven by this force, and by tides and gravity waves that propagate from the lower atmosphere, break and deposit their energy in this region. Lower and upper circulation models (including General Circulation Models) have recently been extended into the middle atmosphere, and need adequate temperature/density data to be validated.

Until recently, there were few temperature profiles measured in the upper atmosphere: Viking lander entry profiles (Seif & Kirk, 1977) and an indirect deriva-

tion above 120 km from Mariner-9 airglow (Stewart et al., 1972). New profiles were derived from Mars Pathfinder (MPF) entry accelerometry (Magalhaes et al., 1999) and Mars Global Surveyor (MGS) aerobraking data (Keating, 1998). The Thermal Emission Spectrometer (TES) on MGS produces 3-D temperature fields up to 35 km in its nadir mode and up to 65 km in the limb-viewing mode (Conrath et al., 1998; 1999). Radio occultation studies from Mars probes result in profiles below 20 km (see Hinson et al., 1999 for recent MPF radio profiles). Ground-based microwave observations based on CO-line profiling (Clancy et al., 1990) constrain temperature profiles on large (planetary) scales up to ~50 km. The thermal structure and circulation of this part of the atmosphere is of primary importance on Mars: unlike on Earth, where the circulation in the troposphere is somewhat decoupled from that in the stratosphere, the vertical extension of meteorological phenomena appears to be considerable. In some cases, this extension probably reaches the top of the neutral atmosphere around 120 km (e.g. the Hadley cell during northern winter). The circulation there may even affect the meteorology at much lower altitude (Forget et al., 1996). For instance, the strong warming of the polar-night atmosphere during dust storms is thought to result from an enhancement of the meridional wind between 60 km and 100 km (Wilson, 1997). In fact, this behaviour of the martian atmosphere may limit the performance of the general circulation models and thus our understanding of martian meteorology. How can we account for these upper atmospheric processes? Is the lower thermosphere circulation of importance? Because of their limited vertical coverage (< 65 km), TES and similar instruments will not solve the problem, leaving SPICAM as the single optical spectrometer covering this altitude range.

Gravity waves have small vertical wavelengths relative to their horizontal scales, which makes them well adapted for detection by SPICAM. In addition, SPICAM will allow us to observe the propagation and the breaking of these waves up to high altitude for the first time.

2.5 Impact of aerosols on the martian climate

Dusty and volatile aerosols are important components of the martian atmosphere. The strong involvement of the aerosols in basic climate fields means that the lower atmosphere may be considered as a ‘dusty climate’ system. A permanent haze exists with a column optical depth from 0.1 to 1 depending on season, with sporadic increases up to several units during great dust storms. It is known to control temperatures in the troposphere and lower stratosphere. Heating and cooling by aerosols drive dynamical phenomena, varying on scale from general circulation to local waves that give rise to atmospheric turbulence. The contents and distribution of aerosols in the atmosphere are, in turn, controlled by atmospheric motion, being included in the complex feedback that makes the current climate of Mars extremely variable. Volatile aerosols also affect the thermal field by changing the optical properties and settling rates of particles, and therefore provide strongly non-linear thermal feedback determined by the saturation curve. This effect is expected to be most significant during aphelion (Clancy et al., 1996; Rodin et al., 1999).

Exploring the phenomena described above implies detailed studies of the vertical, lateral and size distribution of mineral and volatile aerosols, as well as water vapour, in the lower atmosphere. SPICAM’s large wavelength range (0.12-1.7 μm) provides a unique opportunity to study micron-sized aerosols at high spatial resolution. Simultaneous high-resolution measurement of the water vapour profile yields data on microphysical condition of cloud formation, e.g. the degree of supersaturation in the stratosphere and water eddy transport rates in both gaseous and condensed phases. Comprehensive modelling of thermal balance, turbulent transport and microphysics of water vapour, ice and dust interaction with a self-consistent 1-D model (Rodin et al., 1999) will support these measurements.

The components of the martian atmosphere to be measured by SPICAM are given in Table 1.

Table 1. Components of the martian atmosphere measurable by SPICAM.

Species	*Scientific objective*	*Mode*	*Spectral range*	*Accuracy*	*Altitude range*
O_3	concentration vertical profile	stellar/solar occultation	220-300 nm	2-10%	10-50 km, Δz < 1 km
O_3	total abundance	nadir	220-300 nm	5% (> 0.15 µatm)	ground res 4×4 km
CO_2	atmospheric density and temperature vertical profile	solar/stellar occultation	180 nm	2-10% 5K	20-160 km, Δz < 1 km
CO_2	surface pressure, tides	nadir	200 nm 1.43 µm	0.2 mbar 0.1 mbar	n/a
H_2O	total abundance	nadir	1.38 µm	0.2. pr. µm (detectable)	ground res 5×5 km
H_2O	concentration/vertical profile	solar occultation	1.1, 1.38 µm	see text	5-30 km (clear atm.) 20-50 km (dusty atm.) Δz = 2-3km
D, H	isotope ratios	limb emission	121 nm	20%	
Aerosols	vertical profile of characteristics mapping of characteristics	solar/stellar occultation nadir spectropolarimetry	UV-IR 1.0-1.7 µm	10^{-3} (photometry) polarisation rejection 10^{-4}	5-60 km, Δz = 2-3 km exploratory
O_2	concentration vertical profile	stellar occultation	200 nm	20%	35-90 km never done before
O_2	concentration	limb emission	1.27 µm		tentative
H_2O_2	total abundance	nadir	210 nm		never done before
SO_2	total abundance	nadir	220 nm		tentative
H, C, O, CO_2^+,CO	vertical profiling of aeronomic emissions	limb emission	118-320 nm	20%	80-400 km, Δz ~ 2 km
Soil	contribution to surface studies	nadir spectropolarimetry	1.0-1.7 µm	10^{-3} (photometry)	ground res 5×5 km

Table 2. SPICAM mass, power and telemetry budgets.

Mass	Electronics block (DPU)	0.9 kg
	Sensor unit (SU)	3.8 kg
	Total	4.7 kg
Power	DPU+SUV	13 W
	DPU+SUV+SIR	18 W
Data volume		
per measurement	SUV	3.1 kB
	SIR	1.05 kB
per orbit		~ 5 MB

3. The Instrumentation

3.1 Overview

SPICAM (Figs. 2-5) consists of two blocks: a sensor unit (SU) that includes UV (SUV) and near-IR (SIR) spectrometers, and a simple data processing unit (DPU). The SOIR solar occultation package (Bertaux et al., 2001) was excluded because of mission mass constraints, but the UV and IR channels have solar occultation capability in their limited wavelength ranges. The instrument's mechanical layout is shown in Fig. 1. Mass, power and telemetry budgets are summarised in Table 2.

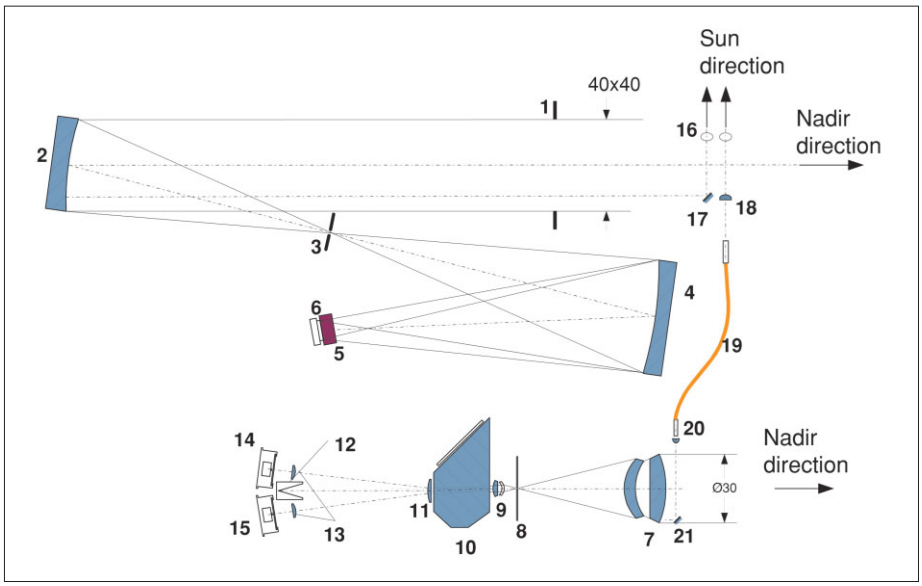

Fig. 2. Optical scheme of SPICAM's UV and IR channels. 1: aperture blend of the UV channel; 2: off-axis parabolic mirror; 3: slit (can be changed from wide to narrow, by a mechanical actuator, see text); 4: concave UV grating; 5: intensifier; 6: CCD; 7: IR channel objective; 8: IR FOV diaphragm; 9/11: collimating lens; 10: AOTF crystal; 12: light trap for undiffracted light; 13: detector proximity lenses; 14: 'extraordinary' beam detector; 15: 'ordinary' beam detector; 16: solar opening (closed by shutter when not looking at Sun); 17/21: flat mirror; 18: IR solar entry; 19: optical fibre; 20: fibre collimator.

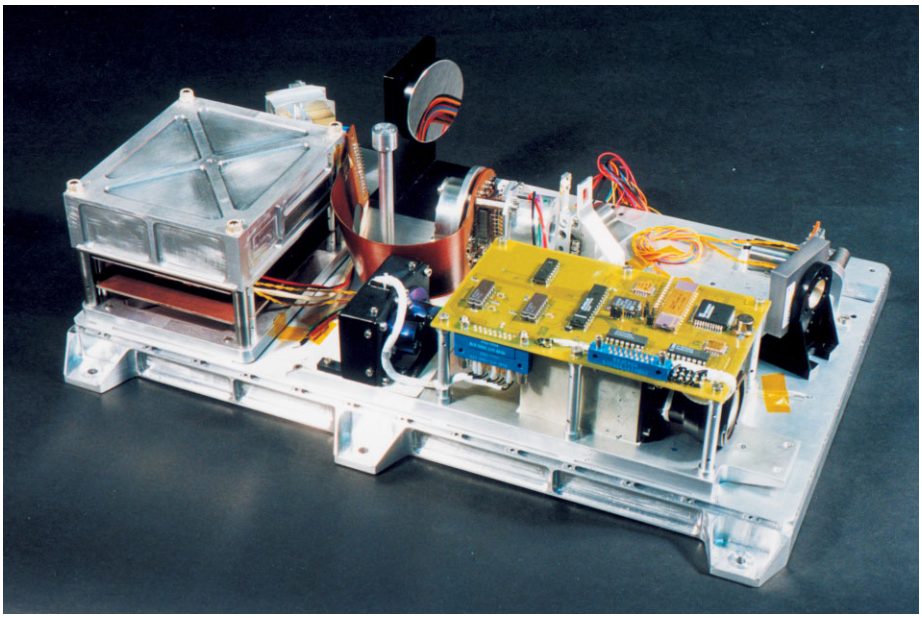

Fig. 3. Breadboard instrument (June 2000; SIR is the prototype), seen from the same vantage point as in Fig. 1. In the final configuration, the parabolic mirror is rectangular, and not circular.

3.2 UV spectrometer (SUV)

The characteristics of the UV spectrometer are summarised in Table 3. For better UV efficiency, SUV includes only two reflective surfaces (Fig. 2). The light flux is collected by an off-axis parabolic mirror, which reflects the light towards the entrance of the spectrometer. At the focal plane, a mechanical slit system provides two configurations: no slit for stellar occultations, and with a slit for extended sources. The slit is divided into two parts, with different widths allowing two spectral resolutions when observing an extended source. The first (50 µm width) gives good resolution with lower flux; the second (500 µm) gives more sensitivity at the expense of a coarser spectral resolution. The slit can be completely retracted, creating a hole corresponding to the total useful field of view of 2×3.16°. This configuration is used in the stellar occultation mode at dark limb when the spectrum of the star is recorded on a few lines of the CCD. The required pointing accuracy is 0.2°.

A holographic concave toroidal grating from Jobin-Yvon, ion-etched for higher

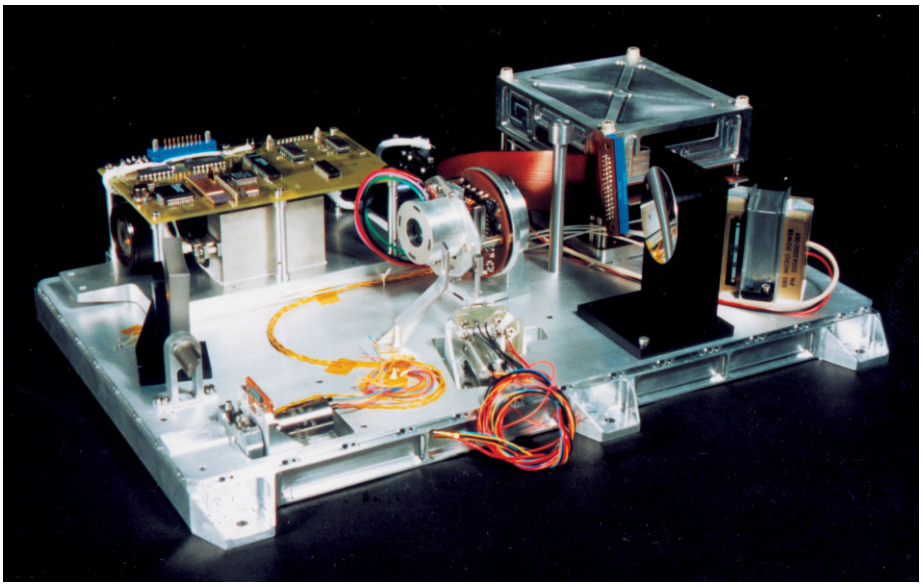

Fig. 4. SPICAM Qualification Model seen from the side of the UV spectrometer. The intensified CCD is placed at the centre. The mirror is at left, the grating is at right.

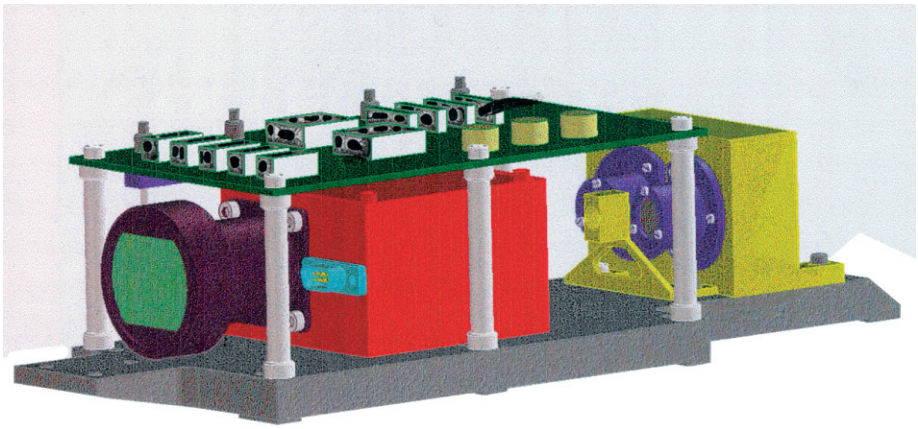

Fig. 5. The AOTF IR channel. From right: entrance lens, AOTF crystal and the two detectors, with the electronics board on top.

Table 3. Characteristics of the SPICAM UV channel (SUV).

Primary mirror	Off-axis parabola 40×40 mm, coated MgF_2, f = 120 mm
Slit	50 µm × 4.6 mm; 500 µm × 2.2 mm
FOV	of a pixel 0.7×0.7´ 2×3.16° no slit (stellar occultation) 0.24×0.95º with double slit
Spectral range	118 - 320 nm
Grating	holographic, concave, toroidal coated MgF_2, 290 lines/mm, blazed 170 nm
Spectral resolution per pixel	0.51 nm
Resolving power (occultations)	120-300 stellar; small slit
Resolving power (extended source)	120-300 small slit,~20 large slit
Pointing accuracy	< 0.2º
Detector	CCD Thomson TH7863 TE cooled at 270K, useful 288×384 pixels, 23×23 µm
Intensifier	Hamamatsu 200M, solar blind CsTe photocathode, input window MgF_2 + sapphire
Vertical resolution	< 1 km (occultations), ~10 km (limb)

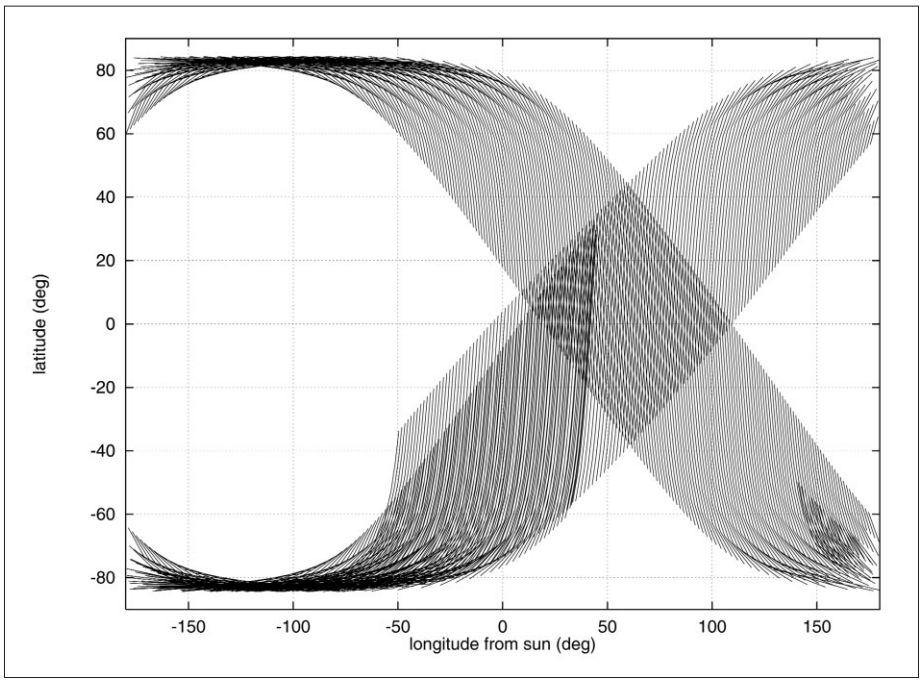

Fig. 6. Longitude from the Sun around pericentre (spacecraft altitude below 800 km) during the first martian year of the mission. (Figure adopted from Hechler & Yanes, 1999).

efficiency, feeds the detection block. The image ratio is ~1, which means that a monochromatic image in the entrance of the spectrometer is conserved in the plane of the detector. The spectral resolution for a point source determined by aberrations is about 1 nm. The CCD detector is a Thomson TH7863 with 288×384 useful pixels and a masked zone of equivalent size. Pixel size is 23×23 µm. The detector is electrically cooled to ~0°C, where the dark current equals 800 electrons per pixel per second, or a few ADU (Analogue to Digital Unit) only. By means of custom-made fibre optics, the CCD is coupled with the output window of the image intensifier (from Hamamatsu, type 200M). A solar blind CsTe photocathode has zero quantum efficiency beyond 320 nm. The input window is made of MgF_2 in order to reach down to Lyman-α (a target of SPICAM). An additional sapphire filter is glued above the window and covers it in part, preventing overlapping of diffraction orders and Lyman-α stray light.

3.2.1 Expected performances

Taking into account the optical characteristics of the UV spectrometer components, quantum efficiency of the photocathode, star spectrum and its reddening owing to interstellar dust absorption, the S/N ratio of SUV in stellar occultation mode can be estimated. Adopting the equation of Henry, it was found that there are nine stars emitting more than 10^4 phot. s^{-1} cm^{-2} nm^{-1} at 220 nm, and 86 stars emitting 10^3-10^4 phot. s^{-1} cm^{-2} nm^{-1}. For these two thresholds, S/N is respectively > 91 and > 29 per pixel. There are ~100 pixels that may be used to determine the CO_2 or ozone absorption, and this gives an idea of the likely accuracy achieved on the retrieval of line density of CO_2 and O_3. Simulation exercises show that the accuracy should be of the order of 2-10% for CO_2 (20-160 km) and ozone (below 50 km).

For an extended source observation, the whole slit is illuminated, and it is possible to integrate over several lines of the CCD. When looking at nadir (dayside), the expected number of photoevents that yield S/N ~ 500 for 1 s integration is 2.5×10^5 nm^{-1} at 270 nm.

For limb observations, a typical airglow emission of 8 kR nm^{-1} (as recorded at the bright limb by Mariner-9) results in ~ 4000 photoevents per pixel at 220 nm, yielding a S/N of 62. At wavelengths longer than 300 nm, the large slit would be used for better S/N if necessary. Along the large slit, where the spectral resolution is about

Table 4. Characteristics of the SPICAM near-IR channel (SIR).

Spectral range	1.0-1.7 µm
Spectral resolution	0.5 nm at 1.0 µm; 1.2 nm at 1.7 µm or better than 4 cm^{-1}
FOV	1º
Telescope	Lens type, Ø 30 mm
AOTF	TeO_2, efficiency 70% (in polarised light), aperture 3.6×3.6 mm, ±3.5º
Detector	2 InGaAs PIN diodes (Hamamatsu G5832), Ø 1 mm, 1 stage TE cooled to –15ºC, D ~ 3×10^{13} W^{-1} cm Hz
Transmission of optics	20%
S/N	~1000

5 nm, there is 10 times more flux on each pixel than along the narrow slit. It is possible again to integrate over several lines of the CCD. For 50 lines, it yields ~10^4 photoevents per nm at 270 nm, or a S/N of 100 for 1 s integration.

For solar occultations, a 0.2 cm^2 mirror looking 90º from the main optical axis is positioned at the entrance pupil, and the detector operates at the lowest gain and integration time of 10 ms.

3.3 Near-IR spectrometer (SIR)

A single-pixel detector of InGaAs, associated with an AOTF, will allow the measurement of the H_2O column at nadir for an instrument mass of only 0.7 kg. The new AOTF devices are based on Bragg diffraction of an entrance beam by the ultrasonic acoustic wave excited within a crystal. They offer the potential of reaching a resolving power, $\lambda/\Delta\lambda$, superior to 1000, amply sufficient to measure nadir H_2O by scanning the absorption lines at 1.38 µm in the solar reflected spectrum. There are no moving parts such as a chopper. This new concept for IR spectroscopy has not flown before on a civil spacecraft but it is now sufficiently mature for space research application.

The AOTF near-IR spectrometer (SIR) is included alongside the UV package; the optical scheme is shown in Fig. 2. The principal characteristics of SIR are summarised in Table 4. A lens telescope 30 mm in diameter has a focal ratio of 1:1.9. A circular diaphragm 1 mm in diameter placed in the focal plane of the telescope forms the FOV. A collimator with two small lenses forms a beam into a custom-made TeO_2 AOTF crystal with an active zone of 23 mm. The divergence of the beams inside the crystal is limited to ±5.5°. The linear aperture has the minimal pupil of 3.12 mm in the centre of the crystal and is less than 3.5 mm at the edges. The output system separates the beams for different polarisations; it consists of two lenses, the first compensating for the divergence of the output beam, and the second focusing the light at the detector. There are two detectors and two short-focus proximity lenses, for the ordinary and extraordinary beams, to allow measurement of the polarisation of the incoming light.

For simplicity, SIR uses the same solar entrance as SUV. An optical fibre delivers the light to the SIR objective. The entry optics of this fibre creates the angular FOV of about 4 arcsec. A collimator lens at the output of the fibre and a 45° flat mirror mounted at the baffle of the SIR objective complete the design of SIR's solar entrance.

4. Measurements

4.1 Nadir viewing

SPICAM will obtain the first simultaneous measurements of water vapour and ozone for the martian atmosphere. The vertical column of H_2O and O_3 will be obtained

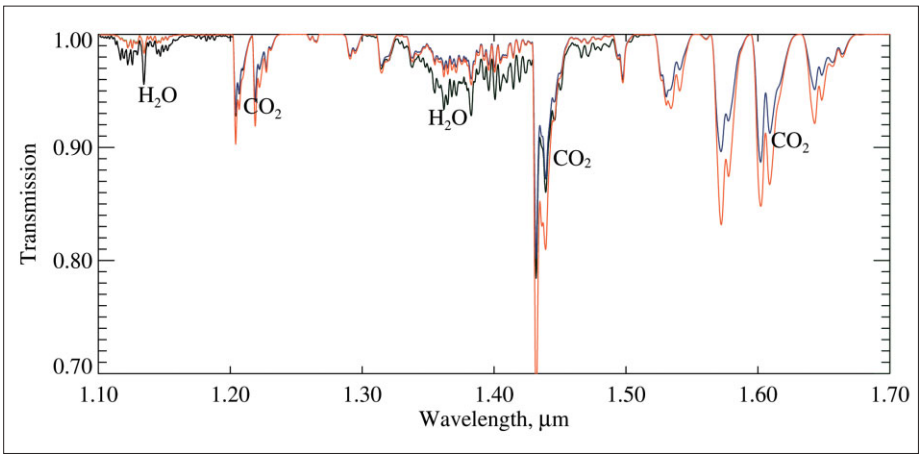

Fig. 7. Line-by-line spectra of nadir atmospheric transmission. Spectra are computed for the water vapour abundance of 15 pr. µm and 50 pr. µm (offset in H_2O bands) and for surface pressures of 6 mbar and 7 mbar (offset in CO_2 bands).

systematically along track, on the dayside, when the spacecraft is nadir-oriented, with a ground resolution of ~4 km at pericentre. The latitude-season coverage for the first year of the mission is presented in Fig. 6. SPICAM will operate up to 15 min before and after pericentre (attitudes up to 1500 km), and its coverage may be denser than is shown in Fig. 6.

4.1.1. Mapping of H_2O total column abundance in the IR

The method of nadir sounding of water vapour in the near-IR bands continues the approach of Mars 3 and MAWD on the Viking orbiters (Farmer & LaPorte, 1972). For Mars Express, the OMEGA instrument will perform spectral mapping in the same spectral range, but H_2O retrievals from these data will be limited because of the much coarser spectral resolution. The principal contribution to water vapour mapping on Mars-Express is expected from the Planetary Fourier Spectrometer (PFS). PFS offers a near-IR range similar to that of MAWD and a thermal-IR range similar to that of Mariner-9's Fourier spectrometer (IRIS). The thermal-IR sounding of H_2O requires a precise knowledge of the temperature profile but it provides redundancy and can be used at night.

SPICAM's observational principle in its nadir mode is the same as that of PFS. SIR's optical axis is parallel to those of all the nadir-looking instruments on Mars Express. SIR's spectral range (1000-1700 nm) requires ~1900 points to be measured. Practically, the amount of data produced by the instrument (polarimetry measurements double the quantity) will be limited by the telemetry budget. The frequency of the AOTF ultrasonic excitation is selected by software, so only the most interesting parts of the spectrum will normally be measured with the desired sampling. The H_2O band could be characterised using only 20 well-chosen points per nadir viewing (FOV 1°), instead of the several thousand for a complete PFS spectrum. The normal exposure time is expected to be within 4 s, allowing the measurement of two spectra (one for each polarisation) of ~300 points each.

Simulated spectra of the atmospheric transmittance in the nadir configuration are shown in Fig. 7. They were computed using the HITRAN-96 database, for a multilayered atmospheric model. The water vapour band at 1.38 µm is apparent. This band is highly suited to H_2O detection because it is strong and almost free from CO_2 influence. For those reasons, it was used by MAWD/Viking (Farmer & LaPorte, 1972). The spectral signatures of H_2O are well resolved at the expected spectral resolution of 4 cm^{-1}. Owing to this relatively high spectral resolution, the gaseous absorption signatures are easy to distinguish from surface spectral features. The estimated nadir S/N will be better than 500, so the minimal detectable amount of H_2O column abundance is well below 1 pr. µm.

SIR is capable of measuring the column abundance of CO_2 in the 1.43 µm band

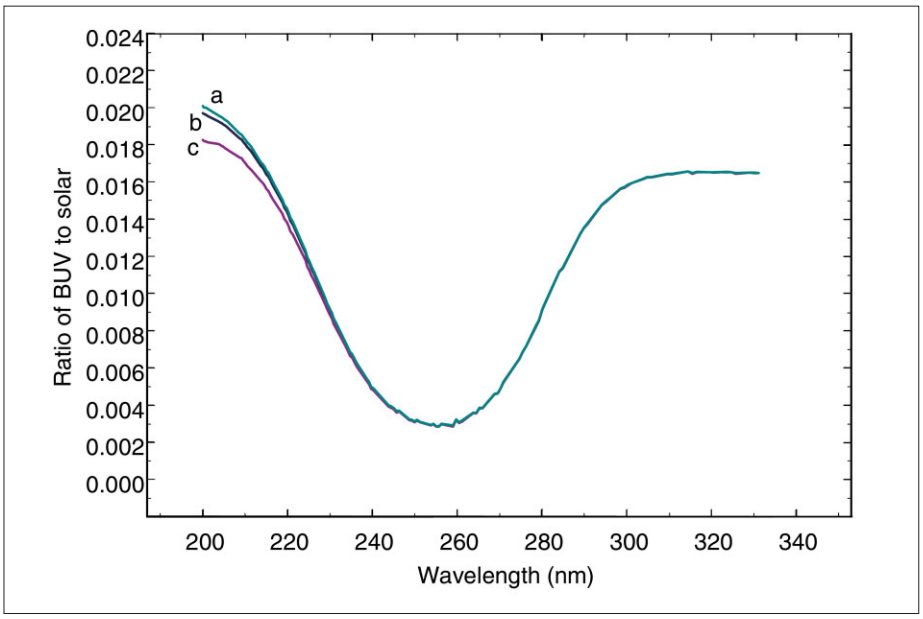

Fig. 8. Modtran computations for nadir geometry. Solar zenith angle 60^0, ozone total abundance 5 µ-atm. A possible effect of H_2O_2 is considered: no H_2O_2 (curve a); H_2O_2 column of 2×10^{16} cm^{-2} (curve b) and 2×10^{17} cm^{-2} (curve c).

and, therefore, the surface pressure. The pressure change from 6 mbar to 7 mbar results in a very large modification of the spectrum (Fig. 7). Combined with the S/N of 1000, it produces an accuracy of better than 0.02 mbar (at least on a relative scale) in the ground pressure. Owing to the AOTF wavelength selection capability, the surface pressure will be measured simultaneously with H_2O, at a very low telemetry budget.

The ordinary and extraordinary beams at the output of an AOTF crystal can be analysed simultaneously using two identical detectors, and the polarisation of the incident light can be measured with high accuracy (Glenar et al., 1994). The second single-element detector does not significantly complicate the instrument. Polarimetry measurements enable a characterisation of grain size for the surface of Mars and of the properties of atmospheric aerosol components (Santer et al., 1985). In particular, it is possible to detect cirrus-like crystal clouds (Lee et al., 1990). With such measurements at a very limited number (2-3) of wavelengths of atmospheric absorption features (e.g. at 1.25 µm and 1.7 µm, see Fig. 7), important additional information about the reflectivity of the surface and the aerosol extinction will be obtained. AOTF's wavelength control means that these measurements will be performed simultaneously with H_2O detection.

Also, the spectral measurements by SIR could be used for cross-validation of OMEGA and PFS data.

4.1.2 Mapping of ozone in the UV

For nadir measurements of ozone, the most sensitive method will be used: the strong Hartley band around 255 nm imprinted on the solar light scattered by the ground and lower atmosphere. This is the technique that discovered ozone on Mars, and it is extensively used on Earth, showing the Antarctic ozone hole. The reflectance UV spectrum results from several sources:

— light reflected by the surface, defined by an albedo *A*, and modified twice by extinction of dust and CO_2 Rayleigh scattering (at $\lambda > 200$ nm);
— light produced by Rayleigh scattering of CO_2;
— solar light reflected by aerosols, distributed vertically;
— absorption by ozone, distributed vertically.

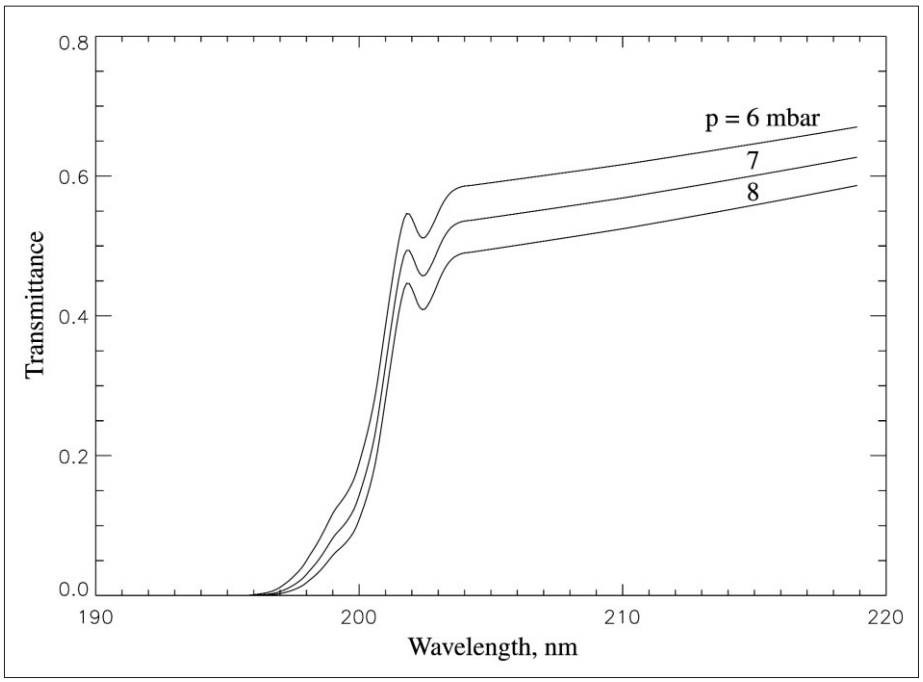

Fig. 9. Variation of the UV nadir transmission spectrum with surface pressure.

Wehrbein et al. (1979) were able to fit the Mariner-9 data with a simple single scattering model, defined by four parameters: ozone optical depth (τ_0), surface albedo (A, assumed to be constant in the UV range), optical depth of dust and Rayleigh (τ_c) and the scale height H_0 of ozone, different from the fixed atmospheric scale height H_S. Indeed, they found a better fit of the bottom of the spectral reflectance trough (Fig. 8) with a ratio $H_0/H_S = 0.6$ than with a fixed value $H_0 = H_S$, showing that ozone was found mostly near the cold surface where the air is dry in high-latitude regions.

A refined analysis scheme requires a more sophisticated algorithm than the one used for the early interpretation of Mariner-7 and -9 data (Barth & Hord, 1971; Barth et al., 1973; Wehrbein et al., 1979) but such algorithms are already working for the Earth (the solar backscatter UV method, used by the Global Ozone Monitoring Experiment on ERS-2).

With SPICAM UV, which registers all wavelengths simultaneously, the S/N will be much greater than for Mariner-9's UV spectrometer (larger than 100 for each nanometer of spectrum in 1 s integration time). This allows the aerosol distribution to be disconnected from the air scale height and Rayleigh scattering. Either a discrete ordinate method or codes similar to those used for interpreting solar backscatter UV spectra in the Earth's atmosphere will be used.

Figure 8, computed for an ozone quantity of 5 µatm (1 µatm = 2.689×10^{15} mol cm^{-2} = 0.1 Dobson units), shows the trough of ozone centred at 255 nm. It is estimated that a trough of ~1% is detectable, corresponding to a vertical optical thickness at 255 nm of 0.5%, or a column density of $N = \tau_0/\sigma = 4\times10^{14}$ mol cm^{-2}, or 0.15 µatm. This allows measurements of ozone in all seasons and latitudes. Above this threshold (say, $N > 2$ µatm), the statistical noise will be a negligible source of error, while systematic errors give an uncertainty of 5%.

SUV will be regularly calibrated in flight by observing standard stars and the Sun. The absolute solar spectrum outside the atmosphere is well known. The reflectance spectrum of Mars will therefore be obtained with a good absolute accuracy and at a spectral resolution of 1 nm. Then, in addition to the main features of the reflection spectrum such as Rayleigh and aerosol scattering overlaid with ozone and CO_2 absorption, other unknowns can be retrieved:

— for surface pressures of 6 mbar and 8 mbar (the total CO_2 vertical column is directly connected to the surface pressure), the absorption edge varies in wavelength position at 210 nm (Fig. 9). Therefore, there is the promising possibility of measuring the surface pressure from the position of the absorption edge in the reflected spectrum. An accuracy of half-a-pixel (easily achievable with such a high S/N) or 0.25 nm on the wavelength would translate into an accuracy of ~0.2 mbar. These data will be used for cross-validation of more precise nadir SIR surface pressure measurements and, combined with the known altimetry, will provide a valuable source for meteorological studies.
— H_2O_2 presents continuous absorption in the UV around 200-220 nm (Yung & Demore, 1999). A simulation of the reflectance (Fig. 8) shows that even for case b, which is not for maximum H_2O_2 conditions, there is a small difference. Though it is difficult to disentangle the continuous absorption by H_2O_2 from dust, it is hoped that a careful analysis with assimilation of aerosol data obtained at other wavelengths will allow the first measurement of this important molecule.

4.2 Vertical profiling by stellar occultation in the UV

SPICAM will measure the vertical distribution of CO_2, temperature, O_3, aerosols, O_2 and possibly H_2O_2 by using stellar occultation, as planned for SPICAM/Mars-96.

The principle is simple. Along the spacecraft's orbit, stars are occulted one after the other by the planetary limb opposite the velocity vector. At a predetermined time, the spacecraft is oriented in such a way that the line of sight of SUV points towards a given star. The stellar spectrum recorded above the atmosphere (say, at 200 km), unaltered by atmospheric absorption, serves as a reference spectrum. Then, while the spacecraft is maintained in a 3-axis, inertial attitude, the line of sight intersects increasingly deeper parts of the atmosphere, down to total occultation.

The stellar occultation technique offers three decisive features:

— an absolute concentration derived from a relative measurement (self-calibration means there is no need for instrument calibration);
— excellent vertical resolution, whatever the distance to the planet (because the star is a point source);
— the accuracy of altitude knowledge, in contrast with limb emission methods, is independent of the spacecraft attitude. The line of sight is determined entirely by the direction of the star in the sky (known) and the position of the spacecraft on its orbit.

Stellar occultations will be performed preferably on the night side of the orbit, and will not affect the operation of dayside mapping instruments. The spacecraft is commanded to direct the SUV line of sight towards a bright UV star and this fixed orientation is maintained within 0.5° (nominal spacecraft capability is better than 0.05°, ensuring that the star remains within the 1° FOV of the instrument during the occultation, which lasts typically 1-4 min). Several (3-5) occultations per orbit are foreseen, the limiting factor being the spacecraft orientation, which is a resource to be shared among the various investigations. Hot stars are preferred, because they are brighter in the UV. Their spectra are flatter than the solar spectrum in the UV. This occultation method offers other features:

— whatever the orbit, there will be numerous opportunities for stellar occultations;
— when a star is occulted during one orbit, it will be occulted again during the following orbits at about the same latitude, but at different longitudes;
— the vertical profiling is not restricted to be along the ground track, in comparison with other instrumental methods;
— de-occultation (star rise) is also possible, since there is no closed-loop tracking system.

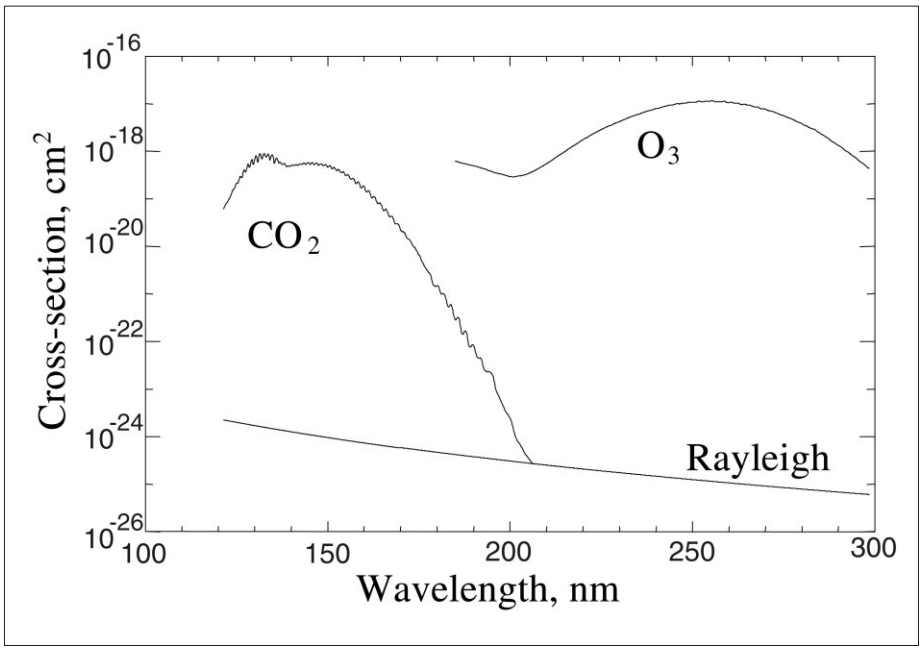

Fig. 10. Absorption cross-sections of CO_2 and ozone in SPICAM's UV spectral range.

Figure 10 shows the absorption cross-sections of CO_2 and ozone in the UV as a function of wavelength. O_2 is absorbing (Schumann-Runge bands) between the peaks of CO_2 and O_3, offering the possibility of actually measuring O_2. Other absorbers are dust (Mie scattering generalised to non-spherical particles) and possibly H_2O_2 and SO_2. The atmospheric transmission simulations are presented in Fig. 11 for various tangential heights. Besides CO_2 and ozone, a dust profile was assumed, with a vertical optical thickness $\tau_d = 0.2$ at 300 nm. Rayleigh extinction by CO_2 was also included in the simulations.

Because the CO_2 cross-section presents an enormous dynamic range in the UV, CO_2 absorption may begin to be detected at an altitude of 150 km. For decreasing tangential heights, the CO_2 manifests itself by a sharp cut-off that increases in wavelength, up to ~200 nm at $z = 10$ km. Longward of 200 nm, the transmission spectrum is dominated by dust and CO_2 Rayleigh extinction, with the additional trough at 255 nm due to ozone. The depth of this trough is a direct measure of ozone line density. From the given S/N in stellar occultation mode (see above), the O_3 line density N_h accuracy will depend on the UV magnitude of the star. It can be estimated that the accuracy on the O_3 line density will be about 2% for about 20 stars in the sky and the measuring threshold corresponding to an absorption of ~1% corresponds to $N_h = 10^{15}$ mol cm^{-2} (horizontal) and local density of 3.5×10^7 cm^{-3} at all altitudes $z > 15$ km (Korablev, Bertaux & Dubois, 2001).

The Rayleigh extinction above 200 nm can be computed from the CO_2 line density determined below 200 nm. The remaining continuous absorption above 200 nm may be attributed to dust/aerosols for a determination of its vertical distribution and spectral characteristics in the UV.

4.2.1 CO_2 density and temperature profile

Once the line density of CO_2 is determined from the transmission spectra, the local density $n(z)$ is determined from an Abel inversion. Then, the hydrostatic equation allows temperature to be determined. As for O_3, the accuracy on the CO_2 line density will be about 2% for 20 stars. The accuracy of the retrieved temperature is estimated to be ±5K in the whole range of altitude, starting at 130-160 km at the top level, while the lowest altitude achieved will depend on the absorption by aerosols or clouds, and will most likely be 5-20 km.

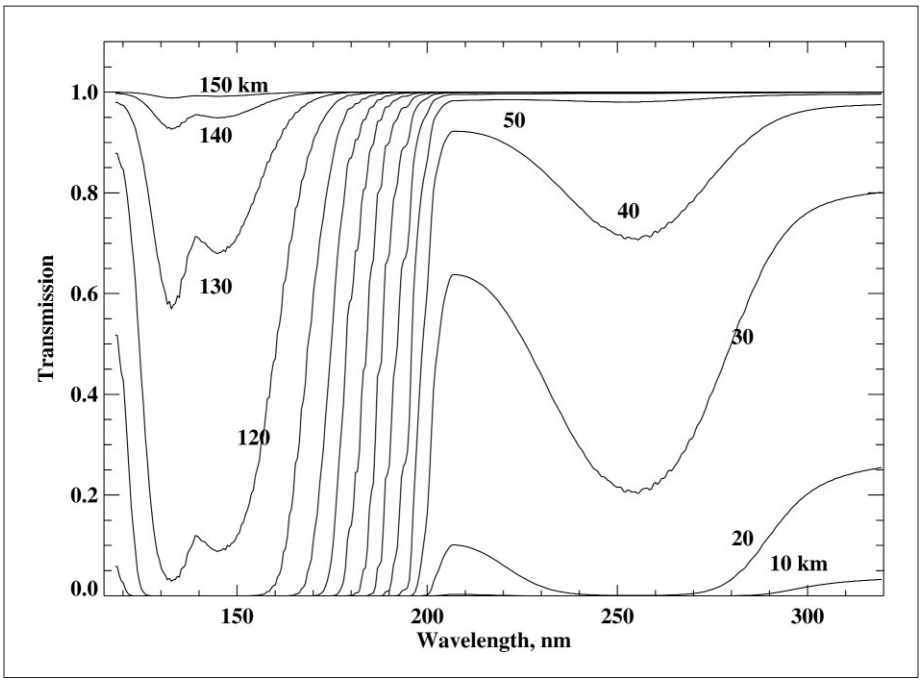

Fig. 11. Simulated stellar occultation transmission spectra for tangential altitudes from 150 km to 10 km in steps of 10 km.

There is a known dependence of the CO_2 absorption cross-section on the temperature T. The retrieval process begins by a first iteration with an *a priori* profile $T(z)$ and corresponding choice of CO_2 cross-section. Then, N and n are retrieved, and the scale height is derived, independently of a wrong choice of the cross-section, providing a new guess for $T(z)$. A few iterations allow convergence of the process. A similar retrieval procedure was developed and tested for the GOMOS/Envisat stellar occultation experiment.

Though nighttime stellar occultations are preferred, it is important to keep in mind that some daytime occultations should be performed on particularly bright stars on the bright limb. They could be combined with UV airglow limb observations to get a better understanding of thermal structure, and to solve unambiguously the discrepancy between Viking and Mariner-9 temperature profiles at $z > 120$ km. In addition, the day-night amplitude variation of the exospheric temperature (at the top of the thermosphere) is a crucial test for the validity of sophisticated Thermospheric General Circulation Models (TGCMs), such as that developed by Bougher et al. (1990). The model predicts a dayside temperature of 270K at 170 km, and a night side T = 160K at the same altitude, but it was impossible to validate this model owing to the lack of measurements. SPICAM offers a wide coverage of density/temperature profiles (local time, season, latitude, geography and solar activity) with which the TGCM could be validated (or invalidated, and modified accordingly). Then, such a model could be used as a predictive tool for managing aerocapture/aerobraking operations in future.

Finally, SUV has a unique ability to detect condensation clouds during the night. The Pathfinder camera detected fog, but was not able to determine the layer's altitude. SUV will do this accurately.

4.2.2 The case for molecular oxygen

Molecular oxygen is the result of CO_2 photodissociation. Its mixing ratio was measured to be of the order of 10^{-3}, and is assumed to be constant. O_2 provides in the Schumann-Runge bands (170-210 nm) an additional absorption that should be measurable. Calculations show that the difference of transmission between an atmosphere with O_2 ($O_2/CO_2 = 10^{-3}$) and an atmosphere without O_2 amounts to 2%

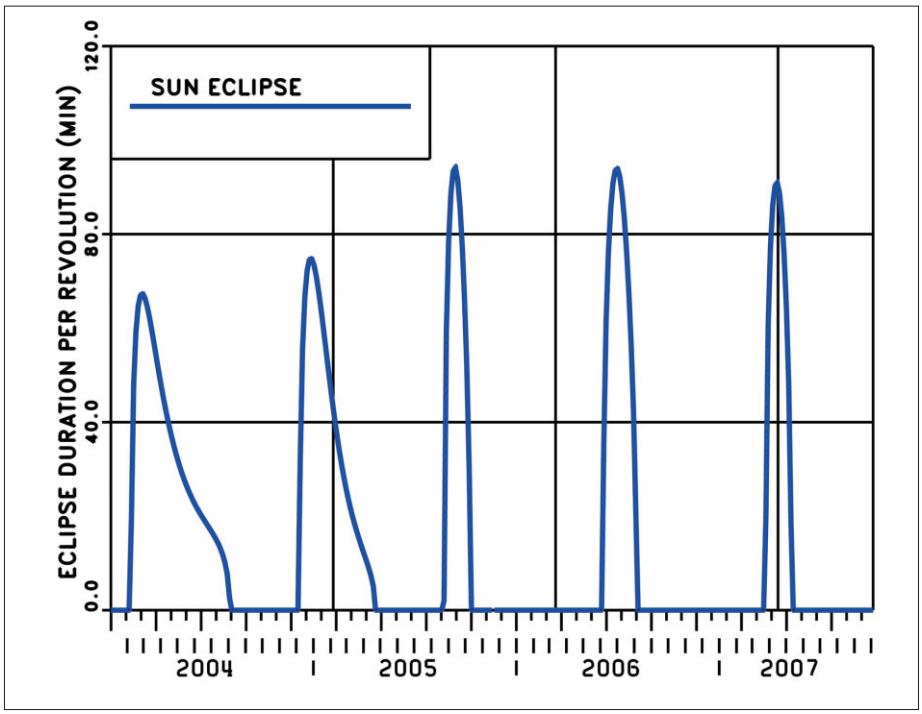

Fig. 12. Periods of solar eclipse for Mars Express orbit G3A. (Figure adopted from Hechler & Yanes, 1999.)

between 80 km and 50 km, in a bandwidth of about 20 nm centred on 190 nm. The absorption decreases somewhat below, but is detectable down to 35 km. In principle, one expects a constant mixing ratio of O_2, in altitude and over the planet, inasmuch as we understand the chemical reactions that control this molecule. There is, however, the special case of the polar winter, when the CO_2 condenses on the martian surface while the O_2 remains, enriching the airmass. The O_2 mixing ratio may be used as a tracer of polar airmass circulation. Its exact value depends on how fast the non-polar airmasses flow to the pole to replenish the locally condensing CO_2 atmosphere. The UV occultation technique is the only way of accessing to this important molecule.

4.3 Solar occultation measurements

As well as the SUV working in the stellar occultation mode, both SUV and SIR will benefit from the advanced pointing capabilities of Mars Express for solar occultations. A solar aperture below the sensor will be pointed towards the Sun by orienting the spacecraft. The angular diameter of the Sun as seen from Mars is 0.35º, but the variability in the brightness of the solar disc requires an attitude control accuracy of 0.1º, well within the spacecraft specifications.

In the case of a polar orbit, there is no precession of the orbital plane. Then, during one martian year, there are two periods of solar occultations, centred on the two dates when the Sun is in the orbital plane (the angle between the solar vector and the orbit plane is zero). Therefore, the possibilities of solar occultation measurements are independent of the other orbital elements.

For the nominal orbit during the mission lifetime, some 700 sunset-sunrise occultation sequences are expected. The occultations occur within about 60 min of pericentre. The two hemispheres are covered twice during spring and autumn (Fig. 12). The spacecraft-limb distance during these periods varies between 4000 km and 11 500 km. The duration of each occultation sequence for the altitude range of 0-150 km is 2-3 min. During the second martian year, there will be fewer occultations closer to apocentre (spacecraft-limb distance above 8000 km).

Solar occultation spectroscopic sounding of a planetary atmosphere offers several advantages. The radiation of the Sun is an incomparably powerful source and it

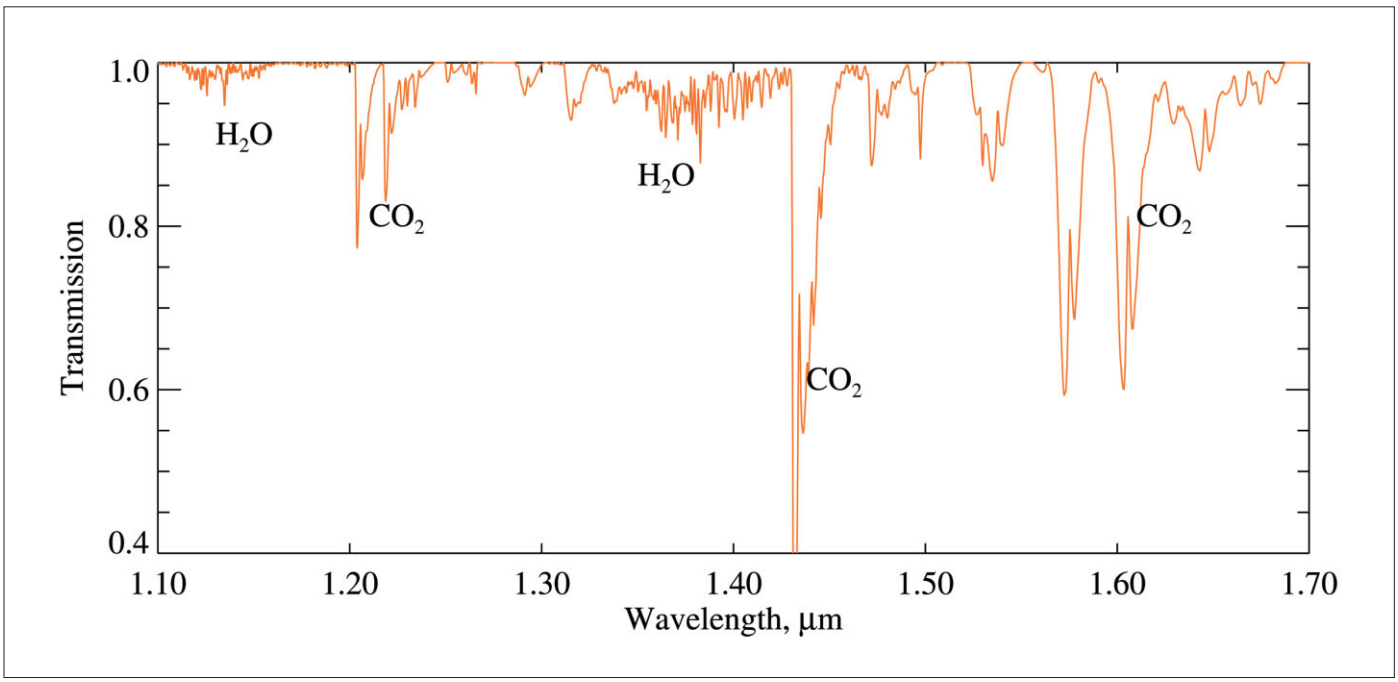

Fig. 13. Simulated near-IR spectrum of the martian atmosphere at the limb (tangential altitude 10 km).

traverses the largest possible atmospheric path (the airmass factor reaches 40-45 for Mars). As for stellar occultations, the measured spectra are compared with the unattenuated signal above the atmosphere, which is measured in the same sequence before occultation to provide self-calibration. A disadvantage is that the atmosphere can be observed only when and where there is a sunset/sunrise.

Vertical resolution of the UV channel is determined by the slit width in one direction and by the pixel height in the other. Assuming that the spectra will be integrated over two lines of the CCD, the FOV will be 1.5×1.5 arcmin, leading to a linear resolution of 1.7-5 km. Using a single CCD line doubles the linear resolution in one direction. The FOV of the IR channel will be better than 4 arcmin because of the fibre optics that deliver the solar light to SIR, limiting the vertical resolution at the limb to 5 km under the best conditions.

The solar-mode SUV will target the same scientific objectives at the terminator as the stellar occultation mode but with a better S/N. The Sun's brightness allows deeper sounding for dusty conditions. The solar mode SIR can measure water vapour vertical profiles – extremely important measurements that cannot be done by any other instrument aboard Mars Express or any planned US mission.

4.3.1 Water vapour profiling by SIR

The efficiency of the solar occultation method for studying the vertical distribution of water vapour was proved during the Phobos mission, when measurements at 1.87 µm determined H_2O vertical profiles in the altitude range 10-50 km (Rodin et al., 1997).

The simulated absorption spectrum of the martian atmosphere at the limb is shown in Fig. 13. It is similar to the nadir spectra, but the absorptions are much more profound. The same near-IR absorption band at 1.38 µm will be used for both. The absorption features of H_2O in this band are deeper than 10%. The accuracy of water-vapour limb sounding depends on atmospheric conditions. Based on available observations (one of which comes from the solar occultation experiment on Phobos, Rodin et al., 1997) and modelling results (Rodin et al., 1999), two types of H_2O profiles can be considered: 'dry and cold' and 'warm and wet'. The dry vertical profile of H_2O constrained by a relatively cold temperature profile in a clean atmosphere (Clancy et al., 1990; Rodin et al., 1997) can be described as 100 ppm below

10 km, ~30 ppm at 15-20 km and 10 ppm above 25 km. In these conditions, the highest sounding altitude is around 30-35 km, and the lowest, constrained by the aerosol absorption, is within 5-10 km. For 'warm and wet' conditions, the highest altitude is 45-50 km (though the absorption at these altitudes is ~0.5%) but the lowest may be 10-15 km because of the larger amount of dust in the atmosphere, which levitates to higher altitudes.

4.3.2 Profiling and characterisation of atmospheric aerosols

The main component of martian aerosols is micron-sized dust, a product of soil weathering, and water ice. According to MGS data (Pearl et al., 1999; Smith et al., 1999), clouds composed of 2 µm particles with visible optical depths of up to 0.1 are formed at the water vapour condensation level, which, in equatorial regions, varies from lower than 10 km at aphelion to almost 50 km in the perihelion season. Occultation spectroscopy is probably the most sensitive remote-sensing technique for directly sounding the vertical structure of clouds and aerosols. In solar occultation, the information about the spectral continuum at distant spectral wavelengths is a byproduct of gaseous absorption retrievals. As soon as the slant atmospheric opacities at different wavelengths are obtained from occultation data, the aerosol extinction can be retrieved by Abel inversion. Then, using the Mie theory (possibly adapted for non-spherical particles), a number of unknown parameters characterising the aerosol component can be extracted, such as the size distribution, and the real and imaginary parts of the refractive index. Also, the vertical variation of key parameters such as the effective size and the number density can be retrieved.

SPICAM measurements are expected to be able to separate the mineral and volatile aerosol fractions. However, when both fractions are present, it will be difficult to determine whether mineral dust particles are cloud condensation nuclei or two kinds of aerosols mixed along the optical path. To help the interpretation, these data will be compared with or assimilated into the 1-D cloud microphysics model mentioned above. It is especially interesting that the vertical profiles of icy aerosols will be obtained in parallel with water vapour profiles. If the observed water vapour is far from saturation, we expect mostly mineral dust aerosols that can be verified by spectroscopic analysis. It is a general assumption that the mineral-dust profile is controlled by the vertical component of large-scale atmospheric circulation and eddy mixing. Therefore, these phenomena can be constrained by the retrieved dust profiles (Korablev et al., 1993).

4.3.3 The consequences of deleting the dedicated solar occultation sensor (SOIR)

The classical IR grating spectrometer for solar occultations (Bertaux et al., 2000) covers a broad spectral range (1.3-4.8 µm) at a relatively high spectral resolution (2-4 cm^{-1}), almost the same as the spectral resolution and FOV of PFS. The AOTF spectrometer has the spectral range of 1.0-1.7 µm and the spectral resolution of ~3.5 cm^{-1}. The FOV in occultation mode is larger (4-5 arcmin) because of the simplified entrance system.

Unfortunately, the mass constraints of Mars Explorer dictated the deletion of SOIR. Apart from the vertical resolution, there is no significant degradation of accuracy for H_2O profiling in solar occultation. No redundancy is lost; only the 1.38 µm H_2O band of the three main short-IR absorption bands (1.38, 1.87, 2.56 µm) will be measured, but the grating spectrometer could measure only one at a time anyway. Reduced spectral resolution does not affect the accuracy drastically. The narrower spectral range makes the aerosol profiling less effective, losing the capacity to measure some interesting components:

— the HDO band at 3.7 µm, so the IR measurements of D/H in the lower atmosphere cannot be compared with the UV measurements in the thermosphere;
— exploratory studies of the carbonic compounds at 3.3-3.7 µm;
— CO measurements in the fundamental CO band at 4.7 µm and in the 2.3 µm

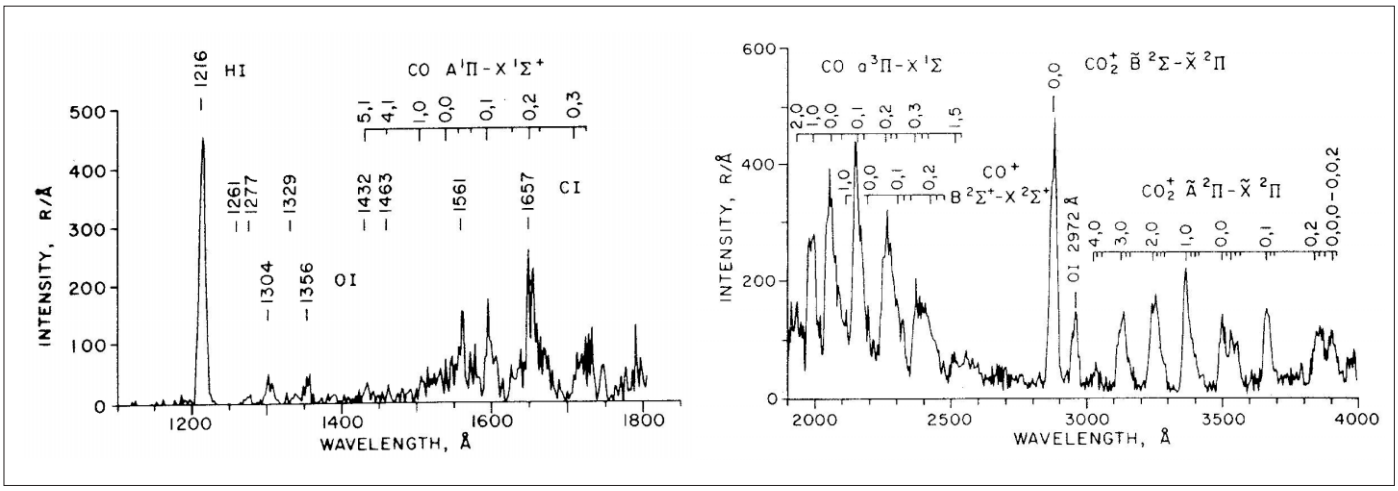

Fig. 14. Mariner-6 and -7 UV spectrum of the upper atmosphere of Mars at a resolution of 20 Å. Limb spectrum at altitudes between 140 km and 180 km, including four individual observations (figure adapted from Barth et al., 1971).

overtone band. Photochemical models predict that CO with its long lifetime would not show any significant altitude stratification, but geographical variability of CO in the lower atmosphere is worth monitoring;

— strong saturated CO_2 bands (at 4.0 µm and 2.7 µm) fall outside of the AOTF spectral range. It was planned to use these bands for atmospheric density studies at 80-120 km; the same sounding will be done in the UV. This redundancy, and the possibility of independently measuring the rotational temperature in the CO_2 bands, is lost.

Conversely, an important advantage of the AOTF spectrometer over the grating spectrometer is that all the interesting regions of the spectral range can be acquired with the desired sampling during the same occultation session using spectral micro-windows (for gaseous components) and distant points (for aerosol characterisation in the spectral continuum). Thus full advantage will be taken of each occultation, which are relatively infrequent events.

4.4 Airglow observations at the limb

4.4.1 Study of the ionosphere in UV

Most of the ionosphere lies below the planned pericentre altitude of Mars Express (300 km) so *in situ* measurements will be impossible. However, the natural UV airglow of the atmosphere allows remote studies of the ionosphere and its temporal behaviour as a function of solar-wind parameters. Figure 14 shows the dayglow spectrum recorded by the Mariner-6 and -7 UV spectrometers (Barth et al., 1971).

The main ionisable neutral constituent is CO_2. The CO_2^+ transition ($B^2\Sigma^{u+} - X^2\pi_g$) at 289 nm is produced by photoionisation of CO_2 from solar UV at $\lambda < 69$ nm. The other band CO_2^+ ($A^2\Sigma_u - X^2\pi_g$), between 300 nm and 400 nm, is produced by a combination of photoionisation and fluorescence scattering on CO_2^+ ions. The SPICAM UV long-wavelength cut-off is at 320 nm, which is sufficient to measure the (4,0) and (3,0) transitions of the A-X band.

The intense Cameron band of CO $a^3\pi - X^1\Sigma^+$ observed at 190-270 nm is produced by a combination of photodissociation of CO_2 by solar UV ($\lambda < 108$ nm), electron impact dissociation of CO_2 and dissociative recombination of CO_2^+. The variation of this band intensity with altitude was used to determine the vertical profile of CO_2 above 120 km, and from the scale height the temperature of the thermosphere was derived (Stewart et al., 1972). This indirect method of determining CO_2 could be validated with SUV, when a stellar occultation is performed on the dayside. The large slit of the FOV will be used to ease the pointing requirement; the bright stellar spectrum would show up, superimposed on the general airglow only on a few lines of the CCD, and the

analysis of the spectro-image would provide information on CO_2: direct measurement by absorptive occultation, and indirect CO Cameron band emission. Neutral O and neutral H vertical density profiles may be derived from the vertical variations of their resonance lines at 130.4 nm and 121.6 nm (Lyman-α), respectively.

4.4.2 Hot oxygen corona, atmospheric escape and D/H ratio

While $CO_2 + h\nu \rightarrow CO_2^+$ is the main photoionisation source, it is the O_2^+ ion that is the most abundant. As a result, a hot atomic oxygen corona around Mars (Ip, 1988), similar to that detected by Venera-11 (Bertaux et al., 1981) around Venus from the emission at 130.4 nm, can be easily detected with SPICAM's better sensitivity. This may be an important source of O escape from the martian atmosphere, somewhat equilibrating the escape of H atoms responsible for the measured enrichment of D/H ratio (a factor of 6) detected in the IR in the lower atmosphere (Owen et al., 1988).

D atoms and H atoms both produce a Lyman-α resonant emission in the upper atmosphere, excited by the H solar Lyman-α line. Since the wavelength separation (H, 121.566 nm; D, 121.533 nm) is larger than the thermal width of each line, the radiative transfer of both types of Lyman-α are totally decoupled. Though SUV has insufficient spectral resolution, these two emissions could be tentatively separated from the vertical distribution of the sum intensities. While the H emission should present a smooth variation around the CO_2 absorption limb (around 120 km), because it is optically thick, the D Lyman-α emission is optically thin, and the intensity doubles just above the limb. Any spike at the CO_2 limb in the vertical distribution of Lyman-α total intensity limb (estimated to be ~300 R) would be due to D atoms. Therefore, both D abundance and H abundance could be determined in the upper atmosphere, and compared with HDO/H_2O measurements in the lower atmosphere in the IR. With Lyman-α measurements from the Hubble Space Telescope, Krasnopolsky et al. (1998) reported that the D/H ratio in the upper atmosphere was lower by a factor of 10 than the D/H ratio in the lower atmosphere. One possible explanation (Cheng et al., 1999) is that HDO is less photo-dissociated than H_2O, because of a smaller cross-section. This effect is probably insufficient to explain the discrepancy, and another explanation is known to be important (Bertaux & Montmessin, 2001): fractionation through condensation. HDO is more prone to condense in ice crystals than is H_2O from the vapour phase, decreasing the D/H ratio with altitude in regions where the photo-dissociation rate is important. This effect is known to play an important role in the Earth's upper troposphere-stratosphere, where HDO is severely depleted just above the tropopause.

4.4.3 O_2 limb airglow in the IR

A dayglow 1.27 µm O_2 ($^1\Delta_g$) emission was observed from the ground at high resolution by Noxon et al. (1976). This emission was predicted just after the discovery of ozone on Mars by Mariner-9 (Barth & Hord, 1971). The martian situation is similar to Earth's, where a strong airglow arises from O_2 ($^1\Delta_g$) production from ozone photolysis. Latitude correlation of this emission with Mariner-9 O_3 was reported by Traub et al. (1979). Mapping of this emission was reported by Krasnopolsky & Bjoracker (2000). Krasnopolsky (1997) argues that the O_2 emission provides even better insight to photochemistry than ozone, since it is more sensitive to the variations of the water vapour saturation level (10-35 km) than total ozone, which remains almost constant.

The band intensity observed by different authors from the ground varies from 1.5 MR to 26 MR; the limb intensity should be greater by a factor of 25 if the dayglow layer is above dust. If, however, the dayglow and dust are uniformly mixed, this factor is approximately 3. A reasonable compromise of these factors is a mean value of ~10. Therefore, if pointed to a sunlit limb together with SUV, SIR could observe the O_2 ($^1\Delta_g$) band intensity of 15-260 MR in a 30 km-thick layer at the limb. This height corresponds roughly to the FOV of the IR spectrometer, and the predicted S/N will be better than 20 in a single spectral bin, or 200-300 for the entire band.

5. Conclusion

Several measurements provided by SPICAM are unique, including:

— ozone measurements are not included on any flying or planned mission. The vertical distribution of ozone will be measured during stellar occultations. H_2O_2 will possibly be detected.
— the density/temperature profiles will provide important constraints for building meteorological and dynamical atmospheric models, from the surface to the exosphere. TES/MGS overlaps up to 80 km altitude, but SPICAM will be the only way to access up to 160 km, the region used for aerocapture and aerobraking. Stellar occultations provide a unique opportunity for detecting clouds on the night side and for measuring O_2.
— the remote sensing of the ionosphere from natural emissions is not included in any other planned mission. The measurements of D/H from UV limb emissions will verify if this ratio is constant or if it varies according to condensation/evaporation processes (as around the terrestrial tropopause).
— after the loss of the Pressure Modulation IR Radiometer on the Mars Climate Orbiter, the only instrument to provide water-vapour vertical profiling will be SPICAM (via solar occultations).

It is already clear that, as on Earth, the atmosphere of Mars has a strong interannual variability. Atmospheric studies must be pursued at every opportunity. It is also essential that a variety of techniques be employed: SPICAM applies the most successful methods from terrestrial studies: backscatter UV spectroscopy and solar/stellar occultation limb sounding.

Acknowledgements
The authors wish to thank M. Richardson, T. Schofield and V. Krasnopolsky for useful discussions. CNES and the Belgian government are financing SPICAM.

References

Atreya, S.K. & Z.G. Gu (1994). Stability of the Martian Atmosphere: Is Heterogeneous Catalysis Essential? *J. Geophys. Res.* **99**, E6, 13,133-13,145

Barth, C.A. & C.W. Hord (1971). Mariner Ultraviolet Spectrometer: Topography and Polar Cap. *Science* **173**, 197-201.

Barth, C.A., C.W. Hord, A.I. Stewart, A.L. Lane, M.L. Duck & G.P. Anderson (1973). Mariner 9 Ultraviolet Spectrometer Experiment: Seasonal Variation of Ozone on Mars. *Science* **179**, 795-796.

Barth, C.A., C.W. Hord, J.B. Pearce, K.K. Kelly, G.P. Anderson & A.I. Stewart (1971). Mariner 6 and 7 Ultraviolet Spectrometer Experiment: Upper Atmosphere Data. *J. Geophys. Res.* **76**, 2213-2227.

Barth, C.A., A.I.F. Stewart, S.W. Bougher, D.M. Hunten, S.J. Bauer & A.F. Nagy (1992). Aeronomy of the Current Martian Atmosphere. In *Mars* (Eds. Kieffer et al.), Univ. of Arizona Press, Arizona, USA, pp1054-1089.

Bertaux, J.L., J.E. Blamont, V.M. Lépine, V.G. Kurt, N.N. Romanova & A.S. Smirnov (1981). Venera 11 and Venera 12 Observations of EUV Emissions from the Upper Atmosphere of Venus. *Planet. Space Sci.* **29**, 149-166.

Bertaux, J.L., D. Fonteyn, O. Korablev, E. Chassefière, E. Dimarellis, J.P. Dubois, A. Hauchecorne, M. Cabane, P. Ranou, A.C. Levasseur-Regourd, G. Cernogora, E. Quemerais, C. Hermans, G. Kockarts, C. Lippens, M. De Maziere, D. Moreau, C. Muller, E. Neefs, P.C. Simon, F. Forget, F. Hourdin, O. Talagrand, V.I. Moroz, A. Rodin, B. Sandel & A. Stern (2000). The Study of the Martian Atmosphere from Top to Bottom with SPICAM Light on Mars Express. *Planet. Space Sci.* **48**, 1303-1320.

Bertaux, J.L. & F. Montmessin (2001). Isotopic Fractionation through Water Vapor

Condensation: the Deuteropause, a Cold Trap for Deuterium in the Atmosphere of Mars. *J. Geophys. Res. Planets* **106**, E 12, 32879-32884.

Blamont, J.E. & E. Chassefière (1993). First Detection of Ozone in the Middle Atmosphere of Mars from Solar Occultation Measurements. *Icarus* **104**, 324-336.

Blamont, J.E., E. Chassefière, J.P. Goutail, B. Mege, M. Nunes-Pinharanda, G. Soushon, V.A. Krasnopolsky, A.A. Krysko & V.I. Moroz (1989). Vertical Structure of Dust and Ozone in the Martian Atmosphere Deduced from Solar Occultation Measurements. *Nature* **341**, 600-603.

Bougher, S.W., C.G. Fesen, E.C. Ridley & R.W. Zurek (1993). Mars Mesosphere and Thermosphere Coupling – Semidiurnal Tides. *J. Geophys. Res.* **98**, 3281-3295.

Bougher, S.W., R.G. Roble, E.C. Ridley & R.E. Dickinson (1990). The Mars Thermosphere. II. General Circulation with Coupled Dynamics and Composition. *J. Geophys. Res.* **95**, 14811-14827.

Carr, M. (1996). *Water on Mars*, Oxford Univ. Press, Oxford, UK.

Chassefière, E., J.E. Blamont, V.A. Krasnopolsky, O.I. Korablev, S.K. Atreya & R.A. West (1992). Vertical Structure and Size Distributions of Martian Aerosols from Solar Occultation Measurements. *Icarus* **97**, 46-69.

Cheng, B.M., E.P. Chew, Ching-Ping Liu, M. Bahou, Yuan-Pern Lee, Yuk L. Yung & M.F. Gerstell (1999). Photo-Induced Fractionation of Water Isotopomers in the Martian Atmosphere. *Geophys. Res. Lett.* **26**, 3657-3660.

Clancy, R.T., D.O. Muhleman & G.L. Berge (1990). Global Changes in the 0-70 km Thermal Structure of the Mars Atmosphere derived from 1975 to 1989 Microwave CO Spectra. *J. Geophys. Res.* **95**, 14543-14554.

Clancy, R.T., A.W. Grossman, M.J. Wolff, P.B. James, D.J. Rudy, Y.N. Billawala, B.J. Sandor, S.W. Lee & D.O. Muhleman (1996). Water Vapor Saturation at Low Altitudes around Mars Aphelion: A Key to Mars Climate? *Icarus* **122**, 36-62.

Conrath, B.J., J.C. Pearl, M.D. Smith & P.R. Christensen (1998). MGS TES Results: Characterization of the Martian Atmospheric Thermal Structure. DPS meeting #30, #11.P06

Conrath, B.J., J.C. Pearl, M.D. Smith & P.R. Christensen (1999). Mars Global Surveyor TES Results: Atmospheric Thermal Structure Retrieved from Limb Measurements. DPS meeting #31, #49.08.

Farmer, C.B. & D.D. LaPorte (1972). The Detection and Mapping of Water Vapor in the Martian Atmosphere. *Icarus* **16**, 34-46.

Forget, F., F. Hourdin & O. Talagrand (1996). Simulation of the Martian Atmospheric Polar Warming with the LMD General Circulation Model. *Ann. Geophys.* **14**, C797.

Fox, G.K., A.D. Code, C.M. Anderson, B.L. Babler, K.S. Bjorkman (1997). Solar System Observations by the Wisconsin Ultraviolet Photopolarimeter Experiment. I. The First Ultraviolet Linear Spectroscopy of Mars. *Astron. J.* **113**, 1152-1157.

Glenar, D.A., J.J. Hillman, B. Saiff & J. Bergstralh (1994). Acouto-optic Imaging Spectropolarimery for Remote Sensing. *Appl. Opt.* **33**, 31, 7412-7424.

Hapke, B. (1981). Bidirectional Reflectance Spectroscopy. I. Theory. *J. Geophys. Res.* **86**, 3039-3054.

Hechler, M & A. Yanes (1999). Mars Express Mission Analysis: the Orbits around G3-A and G3-B. MAS working paper #413. ESOC, Darmstadt.

Hinson, D.P., R.A. Simpson, J.D. Twicken, G.L. Tyler & F.M. Flasar (1999). Initial Results from Radio Occultation Measurements from Mars Global Surveyor. *J. Geophys. Res.* **104**, E11, 26997-27012.

Ip, W.H. (1988). On a Hot Oxygen Corona of Mars. *Icarus* **76**, 135-145.

Jakosky, B.M., R.O. Pepin, R.E. Johnson & J.L. Fox (1994). Mars Atmospheric Loss and Isotopic Fractionation by Solar-wind-induced Sputtering and Photochemical Escape. *Icarus* **111**, 271-288.

Kass, D.M. & Y.L. Yung (1995). Loss of Atmosphere from Mars due to Solar Wind-induced Sputtering. *Science* **268**, 697-699.

Keating, G.M., S.W. Bougher, R.W. Zurek, R.H. Tolson, G.J. Cancro, S.N. Noll,

J.S. Parker, T.J. Schellenberg, R.W. Shane, B.L. Wilkerson, J.R. Murphy, J.L. Hollingsworth, R.M. Haberle, M. Joshi, J.C. Pearl, B.J. Conrath, M.D. Smith, R.T. Clancy, R.C. Blanchard, R.G. Wilmoth, D.F. Rault, T.Z. Martin, D.T. Lyons, P.B. Esposito, M.D. Johnston, C.W. Whetzel, C.G. Justus & J.M. Babicke (1998). The Structure of the Upper Atmosphere of Mars: In situ Accelerometer Measurements from Mars Global Surveyor. *Science* **279**, 1672.

Korablev, O.I., J.L. Bertaux & J.P Dubois (2001). Occultation of Stars in the UV: Study of the Atmosphere of Mars. *J. Geophys. Res.* **106**, 7597-7610.

Korablev, O.I., V.A. Krasnopolsky, A.V. Rodin & E. Chassefière (1993). Vertical Structure of Martian Dust Measured by the Solar Occultation from Phobos Spacecraft. *Icarus* **102**, 76-87.

Krasnopolsky, V.A. (1993). Photochemistry of the Martian Atmosphere (Mean Conditions). *Icarus* **101**, 313-332.

Krasnopolsky, V.A. (1997). Photochemical Mapping of Mars. *J. Geophys. Res. (Planets)* **102**,13,313-13,320.

Krasnopolsky, V.A. & G.L. Bjoracker (2000). Mapping of Mars $O_2(^1\Delta)$ Emission. AGU 2000 Spring meeting, Washington DC, USA.

Krasnopolsky, V.A., O.I. Korablev, V.I. Moroz, A.A. Krysko, J.E. Blamont & E. Chassefière (1991). Infrared Solar Occultation Sounding of the Martian Atmosphere by the Phobos Spacecraft. *Icarus* **94**, 32-44.

Krasnopolsky, V.A., V.I. Moroz, A.A. Krysko, O.I. Korablev, V.S. Zhegulev, A.V. Grigoriev, A.Yu. Tkachuk, V.A. Parshev, J.E. Blamont & J.-P. Goutail (1989). Phobos-2: Solar Occultation Spectroscopic Measurements of the Martian Atmosphere at 1.9 and 3.7 µm. *Nature* **341**, 603-604.

Krasnopolsky, V.A., M.J. Mumma & G.R. Gladstone (1998). Detection of Atomic Deuterium in the Upper Atmosphere of Mars. *Science* **280**, 1576-1580.

Lee, P., S. Ebisawa & A. Dollfus (1990). Crystal Clouds in the Martian Atmosphere. *Astron. Astroph.* **240**, 2, 520-532.

Lellouch, E., G. Paubert & T. Encrenaz (1991). Mapping of CO Millimeter Wave Lines in Mars' Atmosphere: The Spatial Variability of Carbon Monoxide on Mars. *Planet. Space Sci.* **39**, 219-224.

Luhmann, J.G., R.E. Johnson & M.H.G. Zhang (1992). Evolutionary Impact of Sputtering of the Martian Atmosphere by O^+ Pickup Ions. *Geophys. Res. Lett.* **19**, 2151-2154.

Magalhaes, J.A., J.T. Schofield & A. Seiff (1999). Results of the Mars Pathfinder Atmospheric Structure Investigation. *J. Geophys. Res.* **104**, 8943-8955.

Maguire, W.C. (1977). Martian Isotopic Ratios and Upper Limits for Possible Minor Constituents as Derived from Mariner 9 Infrared Spectrometer Data. *Icarus* **32**, 85-97.

McElroy, M.B. (1972). Mars: An Evolving Atmosphere. *Science* **175**, 443-445.

McElroy, M.B. & T.M. Donahue (1972). Stability of the Martian Atmosphere. *Science* **177**, 986.

Moreau, D., A. Marten & Y. Biraud (1998). Meridional and Seasonal Distributions of Trace Gases in the Lower and Middle Atmosphere of Mars. Lunar and Planetary Science Conference, 1998, Houston, TX, USA, Abstract #1369.

Nair, H., M. Allen, A.D. Anbar & Y.L. Yung (1994). A Photochemical Model of the Martian Atmosphere. *Icarus* **111**, 124-150.

Noxon, J.F., W.A. Traub, N.P. Carleton & P. Connes (1976). Detection of O_2 Airglow Emission from Mars and the Martian Ozone Abundance. *Astrophys. J.* **207**, 1025-1035.

Owen, T., J.P. Maillard, C. de Bergh & B.L. Lutz (1988). Deuterium on Mars: The Abundance of HDO and the Value of H/D. *Science* **240**, 1767-1170.

Parkinson, T.D. & D.M. Hunten (1972). Spectroscopy and Aeronomy of O_2 on Mars. *J. Atm. Sci.* **29**, 1390.

Pearl, J.C., M.D. Smith, B.J. Conrath, J.L. Bandfield & P.R. Christensen (1999). Mars Global Surveyor TES Results: Observations of Water Ice Clouds. DPS meeting #31, #76.08.

Rodin, A.V., R.T. Clancy, R.J. Wilson (1999). Dynamical Properties of Mars Water Ice Clouds and their Interactions with Atmospheric Dust and Radiation. *Adv. Space Res.* **23**, 1577-1585.

Rodin, A.V., O.I. Korablev & V.I. Moroz (1997). Vertical Distribution of Water in Near-equatorial Troposphere of Mars: Water Vapor and Clouds. *Icarus* **125**, 21-29.

Roscoe, H.K., R.A. Freshwater, R. Wolfenden, R.L. Jones, D.J. Fish, J.E. Harries & D.J. Oldham (1994). Using Stars for Remote Sensing of the Earth's Stratosphere. *Appl. Optics.* **33**, 7126-7131.

Rosenqvist, J., P. Drossart, M. Combes, T. Encrenaz, E. Lellouch, J.P. Bibring, S. Erard, Y. Langevin & E. Chassefière (1992). Minor Constituents in the Martian Atmosphere from the ISM/Phobos Experiment. *Icarus* **98**, 254-270.

Santer, R., M. Deschamps, L.V. Ksanfomaliti & A. Dollfus (1985). Photopolarimetric Analysis of the Martian Atmosphere by the Soviet MARS-5 Orbiter. I: White Clouds and Dust Veils. *Astron. Astroph.* **150**, 2, 217-228.

Seif, A. & D.B. Kirk (1977). Structure of the Atmosphere of Mars in Summer at Mid-latitudes. *J. Geophys. Res.* **82**, 4364-4378.

Smith, G.R. & D.M. Hunten (1990). Study of Planetary Atmospheres by Absorptive Occultations. *Rev. Geophys.* **28**, 117.

Smith, M.D., J.C. Pearl, B.J. Conrath & P.R. Christensen (1999). Mars Global Surveyor TES Results: Observations of Atmospheric Dust during Mapping. DPS meeting #31, #48.06.

Stewart, A.I. (1972). Mariner 6 and 7 Ultraviolet Spectrometer Experiment: Implication of CO_2^+, CO and O Airglow. *J. Geophys. Res.* **77**, 54-68.

Stewart, A.I., C.A. Barth & C.W. Hord (1972). Mariner 9 Ultraviolet Spectrometer Experiment: Structure of Mars' Upper Atmosphere. *Icarus* **17**, 469-474.

Stoker, C.R. & M.A. Bullock (1997). Organic Degradation under Simulated Martian Conditions. *J. Geophys. Res.* **102**, 10881-10888.

Traub, W.A, N.P. Carleton, P. Connes & J.F. Noxon (1979). The Latitude Variation of O_2 Airglow and O_3 Abundance on Mars. *Astrophys. J.* **229**, 846-850.

Wehrbein, W.M., C.W. Hord & C.A. Barth (1979). Mariner 9 UV Spectrometer Experiment: Vertical Distribution of Ozone on Mars. *Icarus* **38**, 288-299.

Wilson, R.J. (1997). A General Circulation Model Simulation of the Mars Polar Warming. *Geophys. Res. Lett.* **24**, 123-126.

Yung, Y.L & W.D. DeMore (1999). *Photochemistry of Planetary Atmospheres*, Oxford Univ. Press., UK, p.34.